LETTER TO THE EDITOR

Strongly correlated wavefunctions for artificial atoms and molecules

Constantine Yannouleas and Uzi Landman

School of Physics, Georgia Institute of Technology, Atlanta, GA 30332-0430, USA

E-mail: constantine.yannouleas@physics.gatech.edu

Abstract
A method for constructing semianalytical strongly correlated wavefunctions for single and molecular quantum dots (QDs) is presented. It employs a two-step approach of symmetry breaking at the Hartree–Fock level and of subsequent restoration of total spin and angular momentum symmetries via projection techniques. Illustrative applications are presented for the case of a two-electron helium-like single QD and a hydrogen-like QD molecule.

(Some figures in this article are in colour only in the electronic version)

Understanding the nature of strong many-body correlations in condensed-matter finite systems is a fundamental task, which can be facilitated by devising analytical or semi-analytical many-body wavefunctions that approximate well the exact solutions and capture the essential physical properties of such systems. The description of strong correlations in the two-dimensional electron gas in a high magnetic field by the Laughlin wavefunction [1] represents a celebrated example of such a methodology.

Here we construct semianalytical correlated wavefunctions for electrons in two-dimensional single and molecular quantum dots (QDs), which are manmade devices created at semiconductor interfaces and are most often referred to as artificial atoms and molecules (since they contain a finite number of electrons). To this end, we employ a two-step approach consisting of symmetry breaking at the Hartree–Fock (HF) single-determinantal level and subsequent symmetry restoration via projection techniques (PTs) resulting in multideterminantal wavefunctions. PTs were introduced earlier in quantum chemistry [2] for the restoration of the total spin of a molecule and in nuclear physics [3, 4] for the restoration of the total three-dimensional angular momentum (space rotational symmetry) of deformed open-shell nuclei. Our application of these methods to circular single quantum dots (SQDs) requires the simultaneous restoration of both the spin and the angular-momentum symmetries. This requirement poses a more demanding challenge compared to the task of restoring a single broken symmetry, as is the case with the quantum chemistry and nuclear physics many-body problems.

Since the approach of restoration of broken symmetries is largely untested and unknown in the framework of two-dimensional QDs, we aim in this paper at focusing on methodological aspects. For simplicity and conceptual clarity, we construct below strongly correlated wavefunctions for the case of two interacting electrons in an SQD (artificial helium, He-QD) and in a lateral double QD (artificial hydrogen QD molecule, H_2-QDM). Two strongly correlated electrons (with or without an external magnetic field) may exhibit a complex behaviour [1, 5, 6] and can provide the foundation for understanding the properties of a larger number of interacting electrons. Furthermore, the recent growth of interest in quantum computing focused attention on the potential ability to manipulate the ground-state entanglement of two-electron QD systems [7].

The two-body Hamiltonian for two interacting electrons constrained to move on a plane is given by

$$\mathcal{H} = H(\mathbf{r}_1) + H(\mathbf{r}_2) + e^2/\kappa r_{12}, \tag{1}$$

where the last term is the Coulomb repulsion with κ being the dielectric constant of the semiconductor material. $H(\mathbf{r})$ is the single-particle Hamiltonian for an electron in an external perpendicular magnetic field $\mathbf{B}$ and an appropriate potential confinement. For a QDM, the external confinement is given by a two-centre-oscillator potential, and the single-particle Hamiltonian is written as

$$H = T + \frac{1}{2}m^*\omega_0^2(x^2 + y_k'^2) + V_{\text{neck}}(y) + \frac{g^*\mu_B}{\hbar}\mathbf{B} \cdot \mathbf{s}, \tag{2}$$

where $y_k' = y - y_k$ with $k = 1$ for $y < 0$ (left) and $k = 2$ for $y > 0$ (right). x denotes the coordinate perpendicular to the interdot axis (y). $T = (\mathbf{p} - e\mathbf{A}/c)^2/2m^*$, with $\mathbf{A} = 0.5(-By, Bx, 0)$, and the last term in equation (2) is the Zeeman interaction with g^* being the effective g factor, μ_B the Bohr magneton and $\mathbf{s}$ the spin of an individual electron. The shapes described by H are two equal semi-circles connected by a smooth neck ($V_{\text{neck}}(y)$). $-y_1 = y_2 > 0$ are the centres of these semi-circles, $d = y_2 - y_1$ is the interdot distance and m^* is the effective electron mass. The case of a SQD is obtained for $d = 0$, and in this case the confining potential is purely parabolic. For the smooth neck, we use $V_{\text{neck}}(y) = \frac{1}{2}m^*\omega_0^2[C_k y_k'^3 + D_k y_k'^4]\theta(|y| - |y_k|)$, where $\theta(u) = 0$ for $u > 0$ and $\theta(u) = 1$ for $u < 0$. The constants C_k and D_k can be expressed via one parameter, as follows: $C_k = (2 - 4\epsilon^b)/y_k$ and $D_k = (1 - 3\epsilon^b)/y_k^2$, where the barrier-control parameter $\epsilon^b = V_b/V_0$ is related to the actual (controllable) height of the bare barrier (V_b) between the two QDs, and $V_0 = m^*\omega_0^2 y_1^2/2$. The single-particle levels of H are obtained by numerical diagonalization (for details see [10]).

In each case, in the first step of our procedure, the two-electron Hamiltonian (equation (1)) is solved [8–10] in the (symmetry-breaking) spin-and-space unrestricted Hartree–Fock (sS-UHF) approximation; for comparison, the symmetry-adapted restricted Hartree–Fock (RHF) will also be considered. In all cases, we will use $\hbar\omega_0 = 5$ meV and $m^* = 0.067\, m_e$ (this effective-mass value corresponds to GaAs). We will vary the dielectric constant κ, however, in order to control the ratio of the strength of the Coulomb repulsion relative to the zero-point kinetic energy (see in particular the case of the SQD and figure 3 below). The variation of this ratio provides us with the ability to study the whole range of electron correlations, from the regime of weak correlations to that of strong correlations.

We start with the case of a lateral H_2-QDM in a magnetic field, where only the spin projection (SP) needs to be considered, since the confining potential lacks circular symmetry. The example we discuss here[1] corresponds to the case of weak interelectron repulsion (the full

[1] For a systematic study of the H_2-QDM at different values of κ (including $\kappa = 12.9$ (GaAs)) and interdot barrier heights, demonstrating gate control of the entanglement of a pair of electrons, see [10].
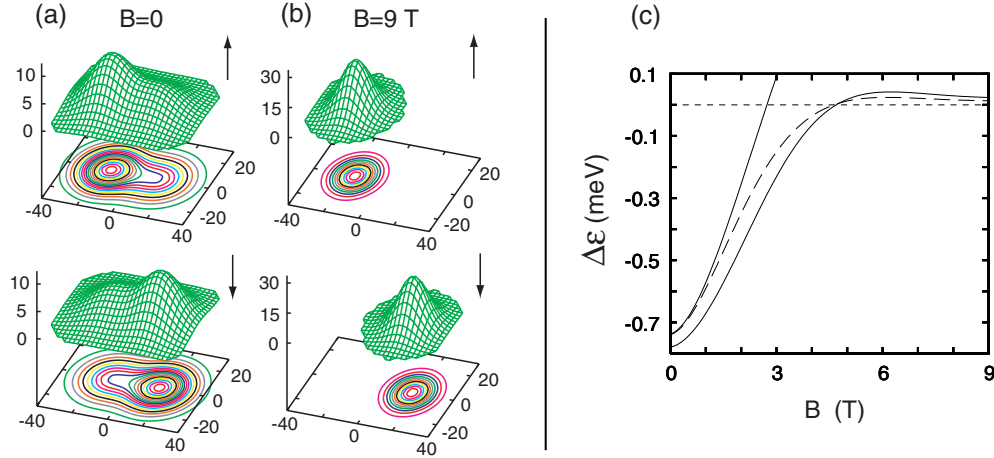
Figure 1. H_2-QDM: the two occupied orbitals (modulus square) of the symmetry-broken 'singlet' sS-UHF solution for (a) $B = 0$ and (b) $B = 9$ T. (c) The singlet–triplet energy difference as a function of an external perpendicular magnetic field and for three successive levels of approximation, i.e. the RHF (top solid curve), the sS-UHF (dashed curve) and the GHL (bottom solid curve). The choice of parameters is: parabolic confinement of each dot $\hbar\omega_0 = 5$ meV, interdot distance $d = 30$ nm, interdot barrier height $V_b = 3.71$ meV, effective mass $m^* = 0.067\, m_e$ and dielectric constant $\kappa = 45$. The effective Zeeman coefficient was chosen as $g^* = 0$; for a small nonvanishing value, like $g^* = -0.44$, the Zeemann splitting does not alter the orbital densities and can be simply added to $\Delta\varepsilon$. Up and down arrows denote spins. Distances are in nanometres and the densities in 10^{-4} nm^{-2}.

choice of parameters is given in the caption of figure 1. The sS-UHF determinant (henceforth we drop the prefix sS in subscripts) which describes the 'singlet' (see below) ground state of the H_2-QDM is given by the expression

$$|\Phi_{\mathrm{UHF}}(1, 2)\rangle = |u(1)\bar{v}(2)\rangle/\sqrt{2}. \tag{3}$$

In equation (3), we have used a compact notation for the Slater determinant with $u(1) \equiv u(\mathbf{r}_1)\alpha(1)$ and $\bar{v}(2) \equiv v(\mathbf{r}_2)\beta(2)$, where $u(\mathbf{r})$ and $v(\mathbf{r})$ are the 1s-like (left) and 1s'-like (right) localized orbitals of the sS-UHF solution, and α and β denote the up and down spin functions, respectively. Such orbitals for the field-free case are displayed in figure 1(a) (left column). Similar localized orbitals (which are complex functions) can appear also in the $B \neq 0$ case (see figure 1(b), right column).

$|\Phi_{\mathrm{UHF}}(1, 2)\rangle$ is an eigenstate of the z-projection of the total spin, $\hat{S} = \hat{s}_1 + \hat{s}_2$, with eigenvalue $S_z = 0$. However, it is not an eigenstate of the square, $\hat{S}^2$, of the total spin (thus the quotation marks in 'singlet' above). From the determinant $|\Phi_{\mathrm{UHF}}(1, 2)\rangle$, one can generate a singlet eigenstate of $\hat{S}^2$ (with zero eigenvalue) by applying the projection operator $P_0 \equiv 1 - \varpi_{12}$, where the operator ϖ_{12} interchanges the spins of the two electrons.

Thus the singlet state of the two localized electrons is given by the projected wavefunction,

$$|\Psi(1, 2)\rangle \equiv P_0|\Phi_{\mathrm{UHF}}(1, 2)\rangle \propto |u(1)\bar{v}(2)\rangle - |\bar{u}(1)v(2)\rangle. \tag{4}$$

In contrast to the single-determinantal wavefunctions of the RHF and sS-UHF methods, the projected many-body wavefunction (4) is a linear superposition of two Slater determinants, and thus it is an entangled state representing a corrective (post-Hartree–Fock) step beyond the mean-field approximation. We notice that the spatial reflection symmetry is automatically restored along with the spin symmetry.

Equation (4) has the form of a Heitler–London (HL) or valence bond [11] wavefunction. However, unlike the original HL scheme which uses the orbitals $\phi_L(r)$ and $\phi_R(r)$ of the separated (left and right) QDs, expression (4) employs the sS-UHF orbitals which are self-consistently optimized for any separation d, interdot barrier height V_b and magnetic field B. Consequently, expression (4) can be characterized as a generalized Heitler–London (GHL) wavefunction. In the context of QDs, the simple HL approach has been proven very useful in demonstrating [7] that the H_2-QDM under an external magnetic field can function as an elemental two-qubit logic gate. Our more accurate GHL approach has the potential of greatly improving the quality of similar investigations regarding the implementation of quantum computing using solid-state nanodevices.

We further notice that our GHL method belongs to a class of PTs known as variation before projection (VBP), unlike the generalized valence bond method familiar in quantum chemistry [12], or the spin-coupled valence bond method [13], which employ a variation after projection (VAP) (see e.g. ch 11.4.2 of [4]). In the context of QDs, a generalization of our GHL approach along the VAP technique may provide even more accurate results. This, however, is left for future work, including the development of the pertinent computer codes.

The energy of a projected state is given [4] in general by the formula

$$E_{PROJ} = \langle \Phi_{UHF} | \mathcal{H} \mathcal{O} | \Phi_{UHF} \rangle / \langle \Phi_{UHF} | \mathcal{O} | \Phi_{UHF} \rangle, \tag{5}$$

where $\mathcal{H}$ is the many-body Hamiltonian and $\mathcal{O}$ is a general projection operator with the property $\mathcal{O}^2 = \mathcal{O}$.

Using the SP operator P_0 in place of $\mathcal{O}$, we find for the total energy, E_{GHL}^s, of the singlet GHL state

$$E_{GHL}^s = \mathcal{N}_s^2 [H_{uu} + H_{vv} + S_{uv} H_{vu} + S_{vu} H_{uv} + J_{uv} + K_{uv}], \tag{6}$$

where H_{uu} etc are the matrix elements of the single-particle Hamiltonian H in equation (1), and J and K are the direct and exchange matrix elements of $e^2 / \kappa r_{12}$. S_{uv} is the overlap integral of the $u(r)$ and $v(r)$ orbitals,

$$S_{uv} = \int u^*(r) v(r) \, dr, \tag{7}$$

and the normalization parameter is given by

$$\mathcal{N}_s^2 = 1/(1 + S_{uv} S_{vu}). \tag{8}$$

At zero magnetic field, the electron orbitals are real functions and equations (6)–(8) reduce to a form familiar from the generalized valence bond theory of quantum chemistry [12].

For the triplet state with $S_z = \pm 1$, the projected wavefunction coincides with the original HF determinant, so that the corresponding energies in all three approximation levels are equal, i.e. $E_{GHL}^t = E_{RHF}^t = E_{UHF}^t$.

In figure 1(c), we display the singlet–triplet energy gap, $\Delta\varepsilon = E^s - E^t$, of the H_2-QDM as a function of the magnetic field B. For all three levels of approximation, $\Delta\varepsilon$ starts from a negative minimum (singlet ground state) and after crossing the zero value it remains positive (triplet ground state). However, after crossing the zero line, the RHF curve incorrectly continues to rise sharply and moves outside the plotted range. After reaching a broad maximum, the positive $\Delta\varepsilon$ branches of both the sS-UHF and GHL curves approach zero for sufficiently large B, a behaviour which indicates that the H_2-QDM dissociates with B. This molecular dissociation can be further seen in the orbitals themselves: at $B = 9$ T (figure 1(b)) the orbitals are well localized on the individual dots, while at $B = 0$ (figure 1(a)) they extend over the entire QDM. Note that, in addition to having the proper symmetry, GHL is energetically the best approximation.
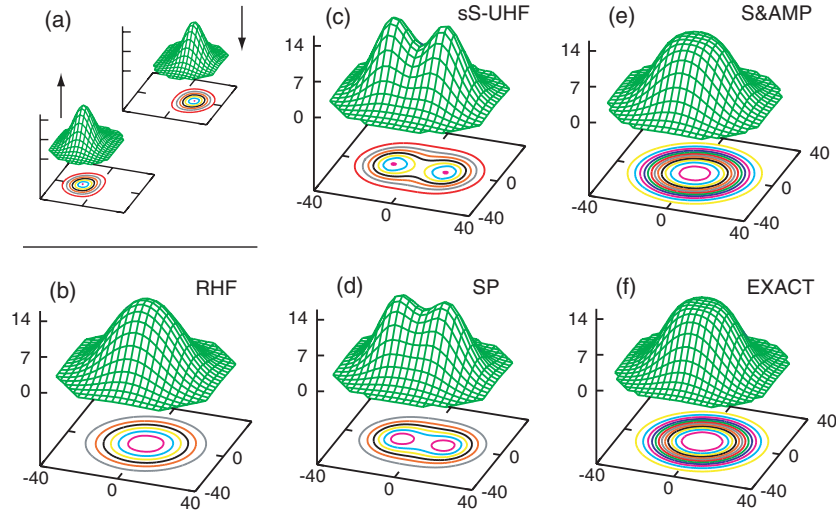
Figure 2. He-QD at $B = 0$: (a) the two occupied orbitals (modulus aquare) of the symmetry-broken 'singlet' sS-UHF solution. The rest of the frames display the electron densities at successive approximation levels, i.e., (b) RHF, (c) sS-UHF, (d) SP alone, (e) S&AMP and (f) exact. See the text for a description of the acronyms. The choice of parameters is: dielectric constant $\kappa = 8$, parabolic confinemenet $\hbar\omega_0 = 5$ meV, and effective mass $m^* = 0.067\, m_e$. Distances are in nanometers and the densities in 10^{-4} nm^{-2}.

We further note that systematic explorations for determining the border of HF instability (i.e. the appearance of broken-symmetry solutions with lower energy) in the case of the H$_2$-QDM are not available. At $B = 0$, this border depends on all four parameters $\hbar\omega_0$, κ, d and V_b. For $\hbar\omega_0 = 5$ meV, $d = 30$ nm and $\kappa = 45$, it was found [10] that this border can be crossed by reducing the interdot barrier V_b to zero. For the same values of B, $\hbar\omega_0$ and d, but for a different $\kappa = 12.9$ (stronger interelectron repulsion, as is the case for GaAs), however, all values of the interdot barrier ($V_b \geqslant 0$) represent cases that lie well within the region of instability.

Next we address the case of two electrons at $B = 0$ in a single QD with a parabolic confinement. As we have shown in earlier publications [8, 9], the sS-UHF solution does not preserve the rotational symmetry for $R_W \geqslant 1.0$ (for $R_W < 1.0$, the sS-UHF solution collapses onto the RHF one). The Wigner parameter R_W expresses the ratio between the interelectron repulsion Q and the zero-point kinetic energy K; it is customary to take $Q = e^2/\kappa l_0$ and $K \equiv \hbar\omega_0$, where $l_0 = (\hbar/m^*\omega_0)^{1/2}$ is the spatial extent of an electron in the lowest state of the parabolic confinement. This gives $R_W \propto 1/(\kappa\sqrt{\omega_0})$, showing that it can be varied through the choice of materials (i.e. κ) and/or the strength of the confinement (ω_0). For $R_W \geqslant 1.0$ and for $S_z = 0$, the sS-UHF yields [9] an infinite manifold of azimuthally degenerate ground-state configurations consisting of two localized antipodal orbitals, suggesting formation of an electron molecule [6, 8, 9] (also referred to as a Wigner molecule). For $\kappa = 8$ ($R_W = 2.39$) and for a specific azimuthal direction (i.e. $\gamma = 0$), the two localized orbitals, $u(\mathbf{r})$ and $v(\mathbf{r})$ with up and down spin, respectively, are depicted in figure 2(a). As was the case with the double-dot example studied above, the $S_z = 0$ sS-UHF determinant $|\Phi_{\text{UHF}}(1, 2)\rangle$ for $\gamma = 0$ is given by equation (3) and thus, in addition to the rotational symmetry, it does not preserve the total-spin symmetry. For the singlet state, one can restore both symmetries successively,

namely, one can generate appropriate projected wavefunctions,

$$|\Psi_I(1,2)\rangle \equiv \mathcal{O}|\Phi_{\text{UHF}}(1,2)\rangle, \tag{9a}$$

by applying the product operator[2],

$$\mathcal{O} \equiv \mathcal{P}_I P_0, \tag{9b}$$

where the SP operator P_0 produces a two-determinant singlet GHL wavefunction as previously explained. The angular-momentum projection operator $\mathcal{P}_I$ yields multideterminantal wavefunctions having good total angular momentum I. This latter operator produces a linear superposition of an infinite number of azimuthal GHL wavefunctions and it is given[3] by [4]

$$2\pi \mathcal{P}_I \equiv \int_0^{2\pi} d\gamma \, \exp[-i\gamma(\hat{L} - I)], \tag{10}$$

where $\hat{L} = \hat{l}_1 + \hat{l}_2$ is the operator for the total angular momentum. In the following we focus on the ground state[4] of the system with $I = 0$.

It is instructive to examine the transformations of the ground-state electron densities (EDs) resulting from the successive approximations, RHF, sS-UHF, SP and combined spin and angular momentum projection (S&AMP). For $\kappa = 8$, such EDs are shown in figure 2. Since the exact solution for two electrons in a parabolic confinement is available [6], we also plot the corresponding ED for the exact ground state in figure 2(f). The EDs of the initial RHF (figure 2(b)) and the final S&AMP (figure 2(e)) approximations are circularly symmetric, while those of the two intermediate approximations, i.e. the sS-UHF and SP, do break the circular symmetry. This behaviour graphically illustrates the meaning of the term restoration of symmetry and the interpretation that the sS-UHF broken-symmetry solution refers to the *intrinsic* (rotating) frame of reference of the electron molecule. We notice that the S&AMP electron density exhibits a characteristic flattening at the top in contrast to the more Gaussian-type RHF one. Thus, although not identical (the exact ED is slightly flatter at the top), the S&AMP ED closely resembles the exact one displayed in figure 2(f). Further, we remark that the SP electron density exhibits in the middle a shallower depression than the corresponding sS-UHF one, in keeping with the fact that the covalent bonding increases the probability of finding the electrons between the individual dots.

Using the projection operator (9b) in the general equation (5), we obtain for the energy $E_{\text{S\&AMP}}$ of the fully projected ground state of the two-electron single QD

$$E_{\text{S\&AMP}} = \int_0^{2\pi} h(\gamma) \, d\gamma \bigg/ \int_0^{2\pi} n(\gamma) \, d\gamma, \tag{11}$$

with

$$h(\gamma) = H_{us} S_{vt} + H_{ut} S_{vs} + H_{vt} S_{us} + H_{vs} S_{ut} + V_{uvst} + V_{uvts}, \tag{12}$$

and

$$n(\gamma) = S_{us} S_{vt} + S_{ut} S_{vs}, \tag{13}$$

$s(\boldsymbol{r})$ and $t(\boldsymbol{r})$ being the $u(\boldsymbol{r})$ and $v(\boldsymbol{r})$ sS-UHF orbitals rotated by an angle γ, respectively. V_{uvst} and V_{uvts} are two-body matrix elements of the Coulomb repulsion[5]. Observe that $E_{\text{S\&AMP}}$

---

[2] In the case of a triplet state, the sS-UHF determinant with $S_z = \pm 1$ preserves the total spin, and thus the application of $\mathcal{P}_I$ alone is sufficient.

[3] The corresponding expression [3] for the three-dimensional angular-momentum projection uses the Wigner functions $\mathcal{D}^I_{MK}(\Omega)$ (see also ch 11.4.6 in [4]).

[4] The family of projected wavefunctions (9) describes all the lowest-energy (yrast band [6]) states with good angular momentum $I = 2, 4, \ldots$, in addition to the ground state ($I = 0$). The yrast-band states with odd values, $I = 1, 3, 5, \ldots$, are generated via a projection of the triplet state.

[5] $V_{uvst} \equiv (e^2/\kappa) \int d\boldsymbol{r}_1 \int d\boldsymbol{r}_2 \, u^*(\boldsymbol{r}_1)v^*(\boldsymbol{r}_2)(1/r_{12})s(\boldsymbol{r}_1)t(\boldsymbol{r}_2)$. In equation (6) $J_{uv} = V_{uvuv}$ and $K_{uv} = V_{uvvu}$.
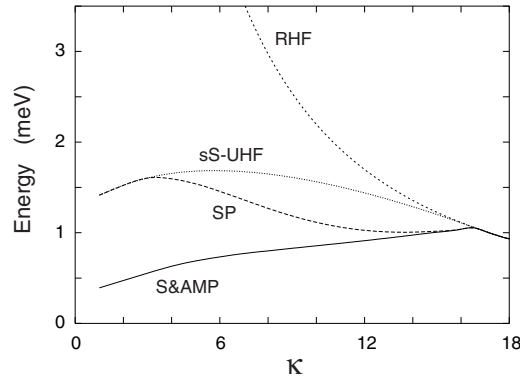
Figure 3. He-QD at $B = 0$: difference between the ground-state energies of various approximations and the exact one, plotted versus the dielectric constant κ. From top to bottom, the curves correspond to the RHF, the sS-UHF, the SP alone and the combined S&AMP approximation. The curve labelled RHF gives the correlation energy. The choice of parameters is: parabolic confinement $\hbar\omega_0 = 5$ meV and effective mass $m^* = 0.067 m_e$.

represents a rotational average over all the possible orientations of the electron molecule and that $h(0)/n(0)$ coincides with the expression (6) for the energy E^s_{GHL} of the covalently bonded H_2-QDM.

To further examine how closely expression (9) describes the ground state of the He-QD, we display in figure 3 the energy deviations of the four approximation steps (i.e. RHF, sS-UHF, SP and S&AMP) from the exact (EX) [6] ground state, as a function of the dielectric constant κ. The variation of κ produces a variation in the strength of the interelectron repulsion, with a larger repulsion (i.e. smaller κ) corresponding to stronger electron correlations.

The correlation energy, $E_{cor} \equiv E_{RHF} - E_{EX}$, is defined as the difference between the RHF ground-state energy and the exact one, and thus it coincides with the top curve in figure 3 denoted as RHF. The ordering (from top to bottom) of the curves in figure 3 reflects the fact that each subsequent approximation step captures successively a larger portion of the total correlations, and thus lowers the total energy. From figure 3, one sees that there are two correlation regimes: in the regime of weak correlations, the three lower curves collapse onto the RHF one; naturally, this regime corresponds to the normal Fermi liquid and extends to $\kappa \to \infty$. The onset of strong correlations and of symmetry-broken HF solutions occurs at $\kappa = 16.5 (R_W = 1.16)$ and extends to $\kappa = 0$.

Note that the percentage, E_{cor}/E_{EX}, of correlations with respect to the exact energy is 6.8 and 49.5% for $\kappa = 16.50$ and 1, respectively. These values are much higher than the values encountered in natural atoms; for this reason, two-dimensional QDs are referred to as strongly correlated systems. Thus it is not surprising that the RHF error in figure 3 grows exponentially for stronger correlations (smaller κ or larger R_W). However, it is remarkable that the S&AMP approximation (where all symmetries have been restored) converges to the exact result for smaller κ. Note that the exact ground-state energy is 19.80 meV for $\kappa = 8$ ($R_W = 2.39$) and 51.83 meV for $\kappa = 1$ ($R_W = 19.09$), resulting for the S&AMP in a relative error of 4 and 0.7%, respectively[6]. These results are in agreement with the experience from nuclear physics, where it has been found [4] that the VBP yields reliable results in the case of strong symmetry breaking (strongly deformed nuclei).

[6] For $\kappa = 8$, the fraction of correlation energy captured by the successive approximations is sS-UHF 44.4%, SP 57.2% and S&AMP 73.1%; the corresponding values for $\kappa = 1$ are 94.5, 94.5 and 98.5%.

Interestingly, the SP curve collapses onto the sS-UHF one for $\kappa \leqslant 3.2$. This behaviour defines [8] an intermediate regime[7] between the Fermi liquid and the regime of strongly crystallized Wigner molecules ($\kappa \leqslant 3.2$). In the latter regime, the overlap (S_{uv}) between the antipodally localized electron orbitals is very small, such that the sS-UHF energy is not effectively lowered by the SP.

We have demonstrated that the sS-UHF method in conjunction with the companion step of restoration of the spin and space symmetries via PTs (when such symmetries are broken) can provide appropriate semianalytical wavefunctions for an accurate description of strongly correlated electrons in artificial atoms and molecules.

References

[1] Laughlin R B 1983 *Phys. Rev. Lett.* **50** 1395
    Laughlin R B 1983 *Phys. Rev.* B **27** 3383
[2] Löwdin P O 1955 *Phys. Rev.* B **97** 1509
    Löwdin P O 1964 *Rev. Mod. Phys.* **36** 966
[3] Peierls R E and Yoccoz J 1957 *Proc. Phys. Soc.* A **70** 381
[4] Ring P and Schuck P 1980 *The Nuclear Many-Body Problem* (New York: Springer) ch 11.4.4
[5] Merkt U *et al* 1991 *Phys. Rev.* B **43** 7320
[6] Yannouleas C and Landman U 2000 *Phys. Rev. Lett.* **85** 1726
[7] Burkard G *et al* 1999 *Phys. Rev.* B **59** 2070
[8] Yannouleas C and Landman U 1999 *Phys. Rev. Lett.* **82** 5325
    Yannouleas C and Landman U 2000 *Phys. Rev. Lett.* E **85** 2220
[9] Yannouleas C and Landman U 2000 *Phys. Rev.* B **61** 15 895
[10] Yannouleas C and Landman U 2001 *Preprint* ArXiv cond-mat/0109167
[11] Heitler H and London F 1927 *Z. Phys.* **44** 455
[12] Goddard W A III, Dunning T H Jr, Hunt W J and Hay P J 1973 *Accounts Chem. Res.* **6** 368
[13] Gerratt J and Lipscomb W N 1968 *Proc. Natl Acad. Sci. USA* **59** 332
[14] Pichard J-L *et al* 2001 *Preprint* cond-mat/0107380

[7] In [8], we referred to the intermediate regime as the weak-Wigner-molecule regime. Such an intermediate regime may also arise in the infinite two-dimensional electron gas at $B = 0$, see [14].